Supporting Information for:

The structure of the extracellular domains of the human interleukin 11 α-receptor elucidates mechanisms of cytokine engagement

Riley D. Metcalfe[1], Kaheina Aizel[1,2], Courtney O. Zlatic[1], Paul M. Nguyen[2,3], Craig J. Morton[1], Daisy Sio-Seng Lio[1,4], Heung-Chin Cheng[1], Renwick C.J. Dobson[1,5], Michael W. Parker[1,6], Paul R. Gooley[1], Tracy L. Putoczki[2,3,7], Michael D.W. Griffin[1].

[1] Department of Biochemistry and Molecular Biology, Bio21 Molecular Science and Biotechnology Institute, University of Melbourne, Parkville, Victoria, Australia,

[2] Inflammation Division, The Walter and Eliza Hall Institute of Medical Research, Parkville, Victoria, Australia

[3] Personalised Oncology Division, The Walter and Eliza Hall Institute of Medical Research, Parkville, Victoria, Australia

[4] Structural Biology Division, The Walter and Eliza Hall Institute of Medical Research, Parkville, Victoria, Australia

[5] Biomolecular Interaction Centre and School of Biological Sciences, University of Canterbury, Christchurch, New Zealand

[6] ACRF Rational Drug Discovery Centre, St. Vincent's Institute of Medical Research, Fitzroy, Victoria, Australia

[7] Department of Medical Biology and Department of Surgery, University of Melbourne, Parkville, Victoria, Australia

This Supporting Information comprises:

Table S1
Figures S1-S10
Movies S1-S4

Table S1. SAXS data collection and analysis.

	IL-11$_{\Delta10}$	**IL-11$_{FL}$**	**IL-11Rα$_{D1-D3}$**	**IL-11Rα$_{D1-D3}$/ IL-11$_{\Delta10}$ complex**
SAXS data collection				
Instrument/source	Australian Synchrotron SAXS/WAXS beamline equipped with Pilatus 2M detector and sheath-flow cell for SEC-SAXS.			
Wavelength (Å)	1.078			
Beam energy (keV)	11.5			
Beam size (µm)	250 × 130			
Sample-to-detector distance (mm)	2038		2539	
q measurement range (Å^{-1}) [a]	0.007-0.664		0.006-0.534	
Absolute scaling method	Comparison with scattering from 1 mm pure water			
Normalization	To transmitted intensity from beamstop counter			
Exposure time	1 s measurements from SEC-SAXS elution			
Sample temperature (K)	293			
SEC-SAXS parameters				
Column	Superdex 200 5/150 Increase			
Flow rate (mL/min)	0.45			
Loading concentration (mg/mL)	5	5	2.2	2.65
Injection volume (µL)	50			
Solvent	20 mM Tris-HCl pH 8.5, 150 mM NaCl, 0.2% sodium azide			
Software employed				
SAXS data reduction	*I*(*q*) vs *q* using Scatterbrain 2.8.2, SEC-SAXS solvent subtraction using *CHROMIXS* from *ATSAS* 2.8.3			
Basic analysis (Guinier, *P(r)*, molecular mass)	*PRIMUS* from *ATSAS* 2.8.3 *GNOM* from *ATSAS* 2.83			
Shape modelling	*DAMMIF* from *ATSAS* 2.8.3 *DAMAVER* from *ATSAS* 2.8.3 *DAMMIN* from *ATSAS* 2.8.3			

Calculation of theoretical intensities	*CRYSOL* from *ATSAS* 2.8.3			
Structural parameters				
Mass from V_c (kDa) (expected mass, ratio to expected, in brackets) [b]	16.3 (18.2, 0.90)	17.2 (19.2,0.90)	33.5 (32.2, 1.04)	50.1 (50.4, 0.99)
Guinier analysis [c]				
R_g (Å)	17.43 ± 0.11	18.89 ± 0.11	30.16 ± 0.32	33.07 ± 0.37
I(0) (cm^{-1})	0.0061 ± 2.4×10^{-5}	0.0068 ± 2.4×10^{-5}	0.011 ± 6.7×10^{-5}	0.0094 ± 6.4×10^{-5}
qR_g min,max	0.18, 1.31	0.21,1.31	0.25, 1.30	0.27, 1.29
P(r) analysis [c]				
R_g (Å)	17.59 ± 0.74	19.00 ± 0.90	31.20 ± 0.14	33.41 ± 0.21
I(0) (cm^{-1})	0.0061 ± 2.1×10^{-3}	0.0068 ± 2.3×10^{-3}	0.0094 ± 5.7×10^{-3}	0.0093 ± 5.1×10^{-3}
D_{max} (Å)	54	61	95	102
Porod volume ($Å^3$)	21700	27600	41200	85500
Shape modelling				
DAMMIF (10 calculations, default parameters)				
q range for fitting (Å)				0.008-0.16
Symmetry, anisotropy assumptions				*P*1, none
NSD (standard deviations)				0.797 (0.100)
χ^2 range				1.035-1.036
Constant adjustment to intensities				8.31×10^{-5}
Resolution (from *SASRES*) [d] (Å)				36
DAMMIN (default parameters)				
q range for fitting (Å)				0.008-0.16

Symmetry, anisotropy assumptions	*P*1, none
χ^2	1.035
Constant adjustment to intensities	8.36×10^{-5}

Atomic modelling

CRYSOL (no constant subtraction)

Structure	PDB ID: 6O4O	PDB ID: 6O4O	PDB ID: 6O4P, chain A, residues 2-297 [e]	Docked model
χ^2	1.43	3.21	1.05	1.03
Calculated R_g (Å)	17.41	17.69	32.17	33.97

SASBDB IDs for data and models:

	SASDGH2	SASDGJ2	SASDGG2	SASDGK2

[a] $q=(4\pi\sin\theta)/\lambda$

[b] (1)

[c] Errors from *AUTORG* or *GNOM*, ± standard deviation

[d] (2)

[e] Corresponding to the residues present in the IL-11R$\alpha_{D1\text{-}D3}$ construct.

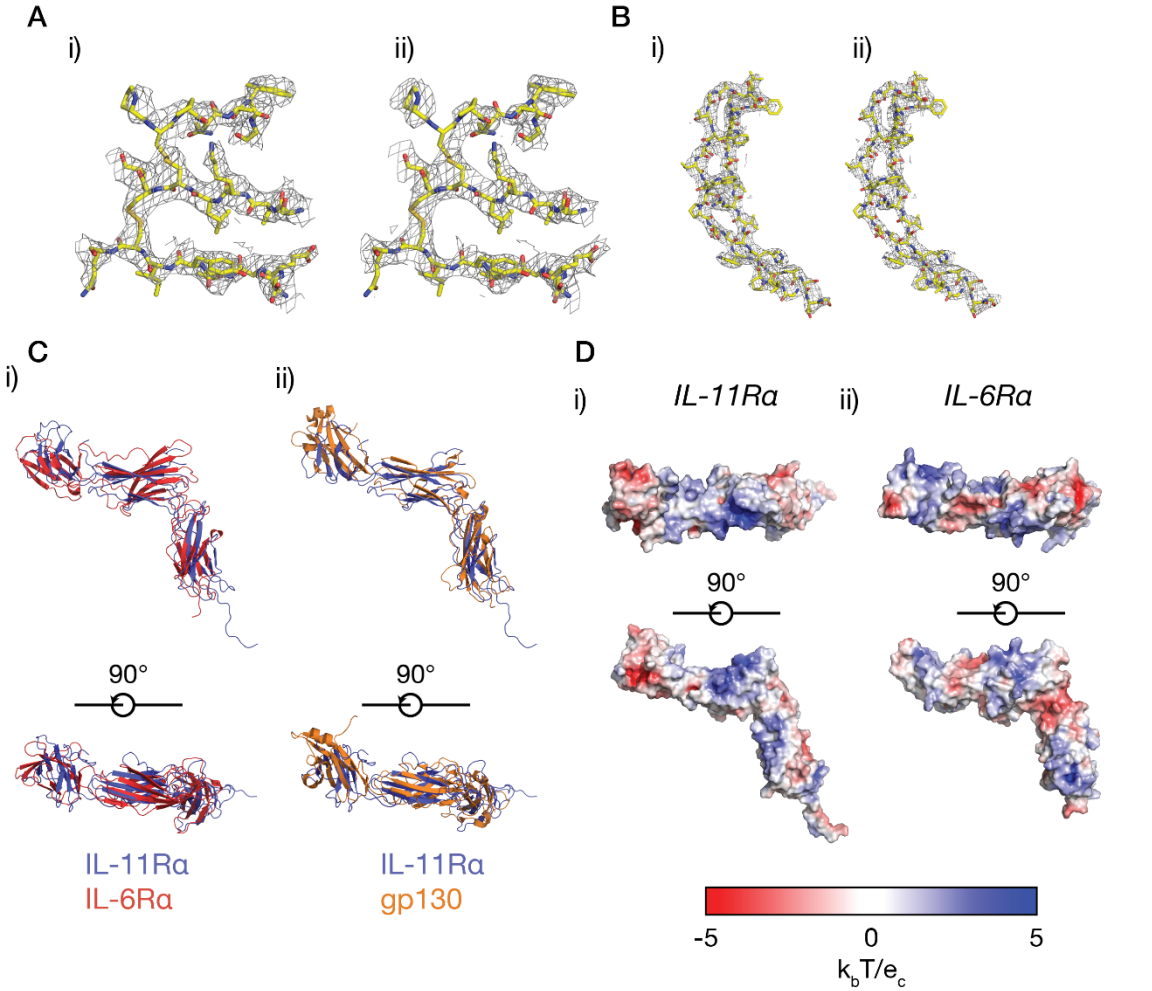
A
i)
ii)
B
i)
ii)
C
i)
ii)
90°
90°
90°
90°
IL-11Rα
IL-6Rα
IL-11Rα
gp130
D
i)
IL-11Rα
ii)
IL-6Rα
90°
90°
-5
0
5
k_bT/e_c

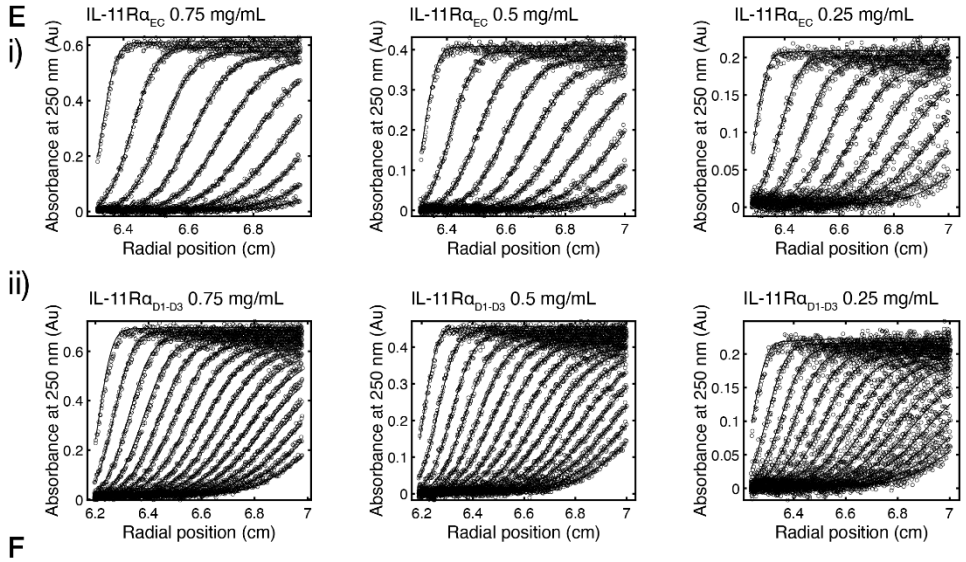
E
i)
IL-11Rα_EC 0.75 mg/mL
IL-11Rα_EC 0.5 mg/mL
IL-11Rα_EC 0.25 mg/mL
Absorbance at 250 nm (Au)
Radial position (cm)
ii)
IL-11Rα_D1-D3 0.75 mg/mL
IL-11Rα_D1-D3 0.5 mg/mL
IL-11Rα_D1-D3 0.25 mg/mL
Absorbance at 250 nm (Au)
Radial position (cm)

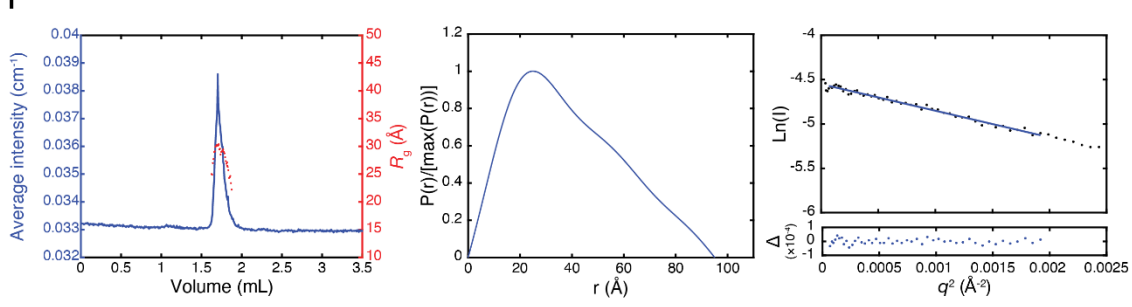
F
Average intensity (cm⁻¹)
R_g (Å)
Volume (mL)
P(r)/[max(P(r))]
r (Å)
Ln(I)
Δ (×10⁻⁴)
q² (Å⁻²)

Figure S1: A) Electron density for the two disulfide bonds in D1 of IL-11Rα (contorted at 1 σ), i) 2Fo-Fc map, ii) simulated annealing composite-omit map. B) Electron density for the WSXWS motif and surrounding residues for D3 of IL-11Rα (contoured at 1 σ), i) 2Fo-Fc map, ii) simulated annealing composite-omit map. C) The cytokine-binding domains of IL-11Rα overlaid with the cytokine-binding domains of (i) IL-6Rα (PDB ID: 1N26) (3), and (ii) gp130 (PDB ID: 1I1R, gp130 chain) (4). D) Surface electrostatics for IL-11Rα, i) and IL-6Rα, ii) (PDB ID: 1N26), calculated using APBS. E) Raw AUC data (circles) overlaid with the best fit to a continuous size distribution [c(s)] model for the distributions shown in Figure 1D and 1E. F) Supporting SAXS data for IL-11R$\alpha_{D1\text{-}D3}$, showing the SEC-SAXS chromatograms, a pairwise distance distribution (P(r)) plot and a Guinier plot, for the data shown in Figure 1E.

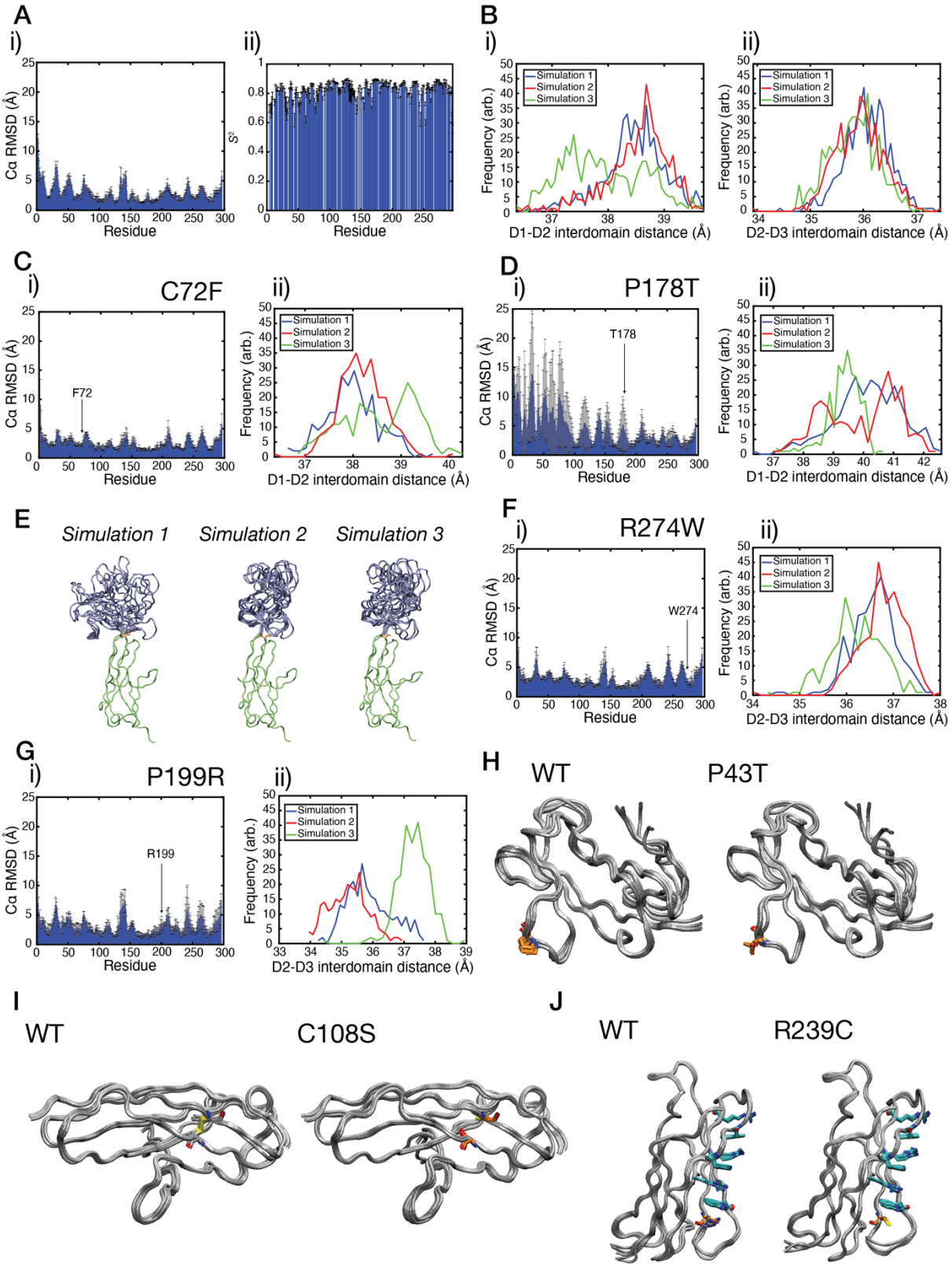

Figure S2: Supporting MD data. A) Cα RMSD and order parameter values for all residues in IL-11Rα. B) i) Interdomain distance distributions for the D1-D2 interdomain distance, and ii) Interdomain distance distributions for the D2-D3 interdomain distance through each of the 50 ns simulations. C) Cα RMSD, i) and D1-D2 interdomain distance distribution, ii) for the C72F mutation. D) Cα RMSD, i) and D1-D2 interdomain distance distribution, ii) for the P178T

mutation. E) Overlay of frames from each of the three MD simulations conducted for the IL-11Rα P178T mutant. F) Cα RMSD, i) and D2-D3 interdomain distance distribution, ii) for the R274W mutation. G) Cα RMSD, i) and D2-D3 interdomain distance distribution, ii) for the P199R mutation. H) Overlay of frames from an MD simulation of the P43T mutation. WT IL-11Rα is shown for direct comparison. I) Overlay of frames from an MD simulation of the C108S mutation. WT IL-11Rα is shown for direct comparison. C98, which forms a disulphide bond with C108 in IL-11Rα is also shown in the figure. J) Overlay of frames from an MD simulation of the R239C mutation. WT IL-11Rα is shown for direct comparison. The other residues in the tryptophan-arginine ladder are shown in cyan. Error bars in all plots are standard deviations, calculated from three 50 ns simulations.

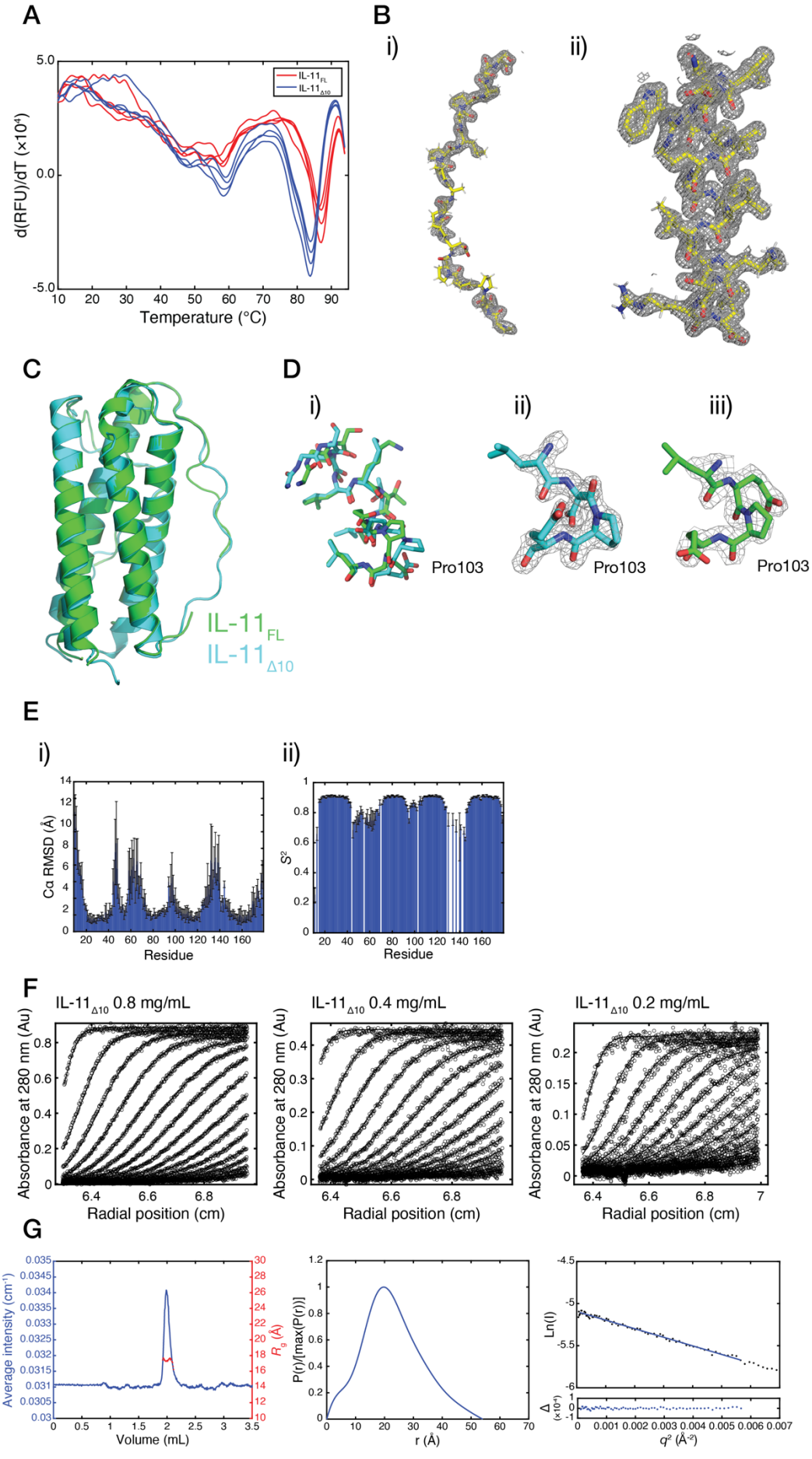
A
B
i)
ii)
C
D
i)
ii)
iii)
Pro103
Pro103
Pro103
E
i)
ii)
Cα RMSD (Å)
Residue
S²
Residue
F
IL-11Δ10 0.8 mg/mL
IL-11Δ10 0.4 mg/mL
IL-11Δ10 0.2 mg/mL
Absorbance at 280 nm (Au)
Radial position (cm)
G
Average intensity (cm⁻¹)
Volume (mL)
P(r)/[max(P(r))]
r (Å)
Ln(I)
q² (Å⁻²)

Figure S3: A) Differential scanning fluorimetry data, showing that IL-11_{FL} and IL-$11_{\Delta 10}$ have very similar thermal stability, and that both are highly stable. IL-$11_{\Delta 10}$ has a temperature of hydrophobic exposure (T_h) of 83.8 °C, and IL-11_{FL} has a T_h of 87.0 °C. B) Representative density for the structure of IL-$11_{\Delta 10}$. i) a portion of the polyproline helix, and ii) a C-terminal portion of helix D. Maps contoured at 1 σ. C) Structural alignment of previous (PDB ID: 4MHL) and current IL-11 structures, showing that they have a similar structure (rmsd 0.5 Å), with a slight difference in position of the A and D helices. D) Comparison of P103 in 4MHL and the structure of IL-$11_{\Delta 10}$. i) an overlay of the 3_{10} helix in both structures, showing the *cis-trans* isomerism exhibited by Pro103, ii-iii) the density supporting the position of Pro 103 in, ii) IL-$11_{\Delta 10}$ and iii), 4MHL (maps contoured at 1.5 σ). E) Cα RMSD and order parameter values for all residues in IL-11 (n=3 100 ns simulations), calculated from the MD simulation. Error bars are standard deviations. F) Raw AUC data (circles) overlaid with the best fit to a continuous size distribution [c(s)] model for the distributions shown in Figure 3G. G) SEC-SAXS chromatogram, a pairwise distance distribution (P(r)) plot, and a Guinier plot for the SAXS data shown in Figure 3H.

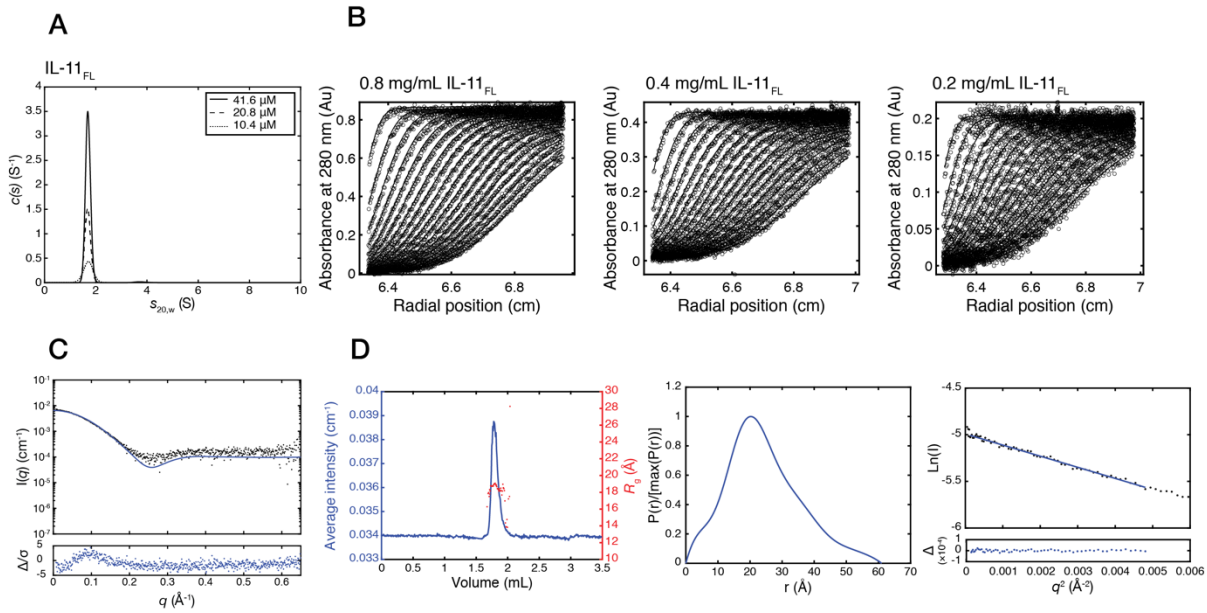

Figure S4: Biophysical characterisation of IL-11$_{FL}$. A) c(s) distributions for IL-11$_{FL}$, at three concentrations, showing that it is monomeric in solution. B) Raw AUC data (circles) overlaid with the best fit to a continuous size distribution [c(s)] model for the distribution shown in (A). C) SAXS data for IL-11$_{FL}$, with the fit to the structure of IL-11$_{\Delta 10}$ overlaid (χ^2 = 3.21). D) SEC-SAXS chromatogram, pairwise distance distribution (P(r)) plot, and Guinier plot for IL-11$_{FL}$.

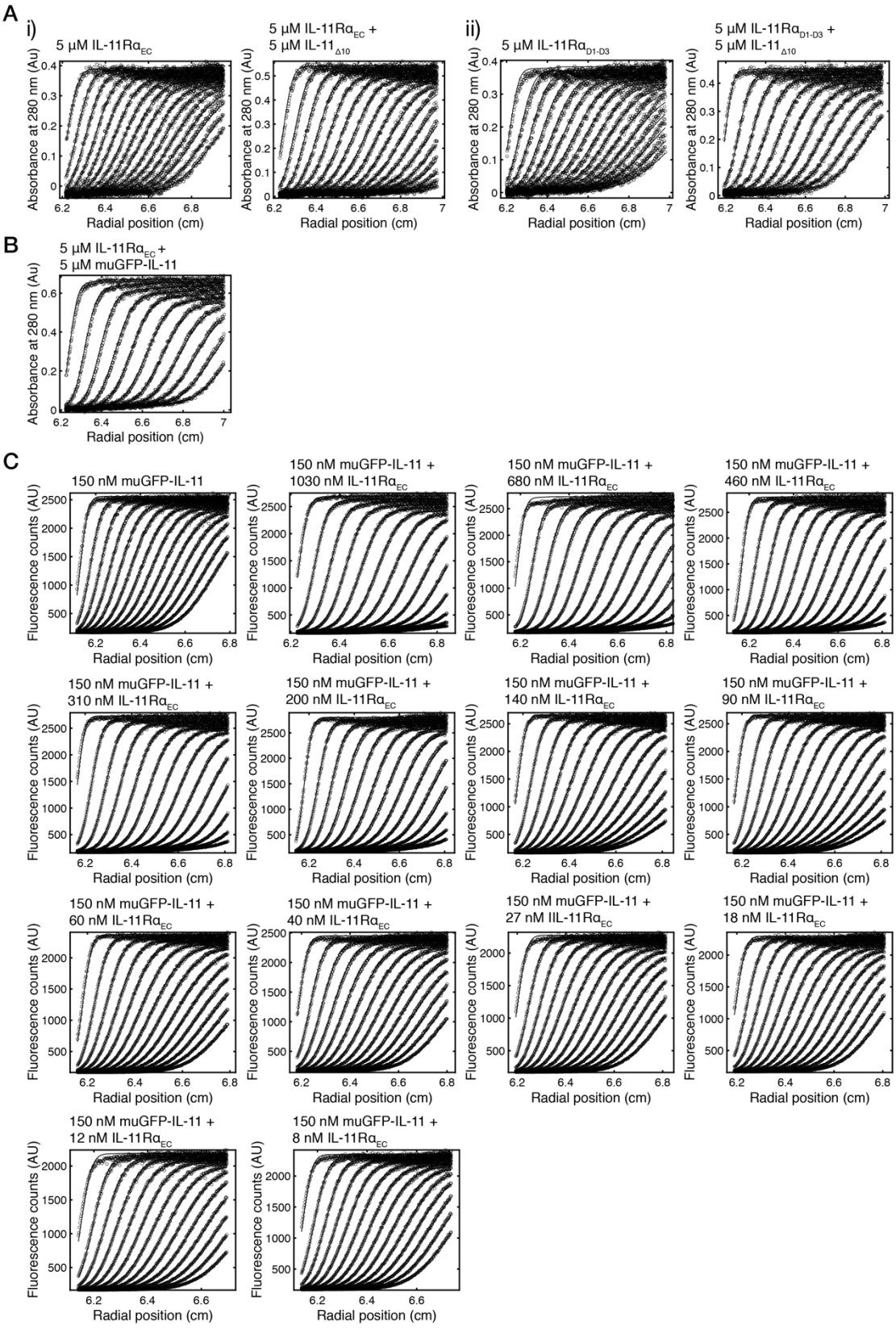

Figure S5: Raw AUC data (circles) overlaid with the best fit to a continuous size distribution [c(s)] model for the distributions shown in, A) i) Figure 4Ai, ii) Figure 4Aii, B) Figure 4B, C) the titration shown in Figure 4D.

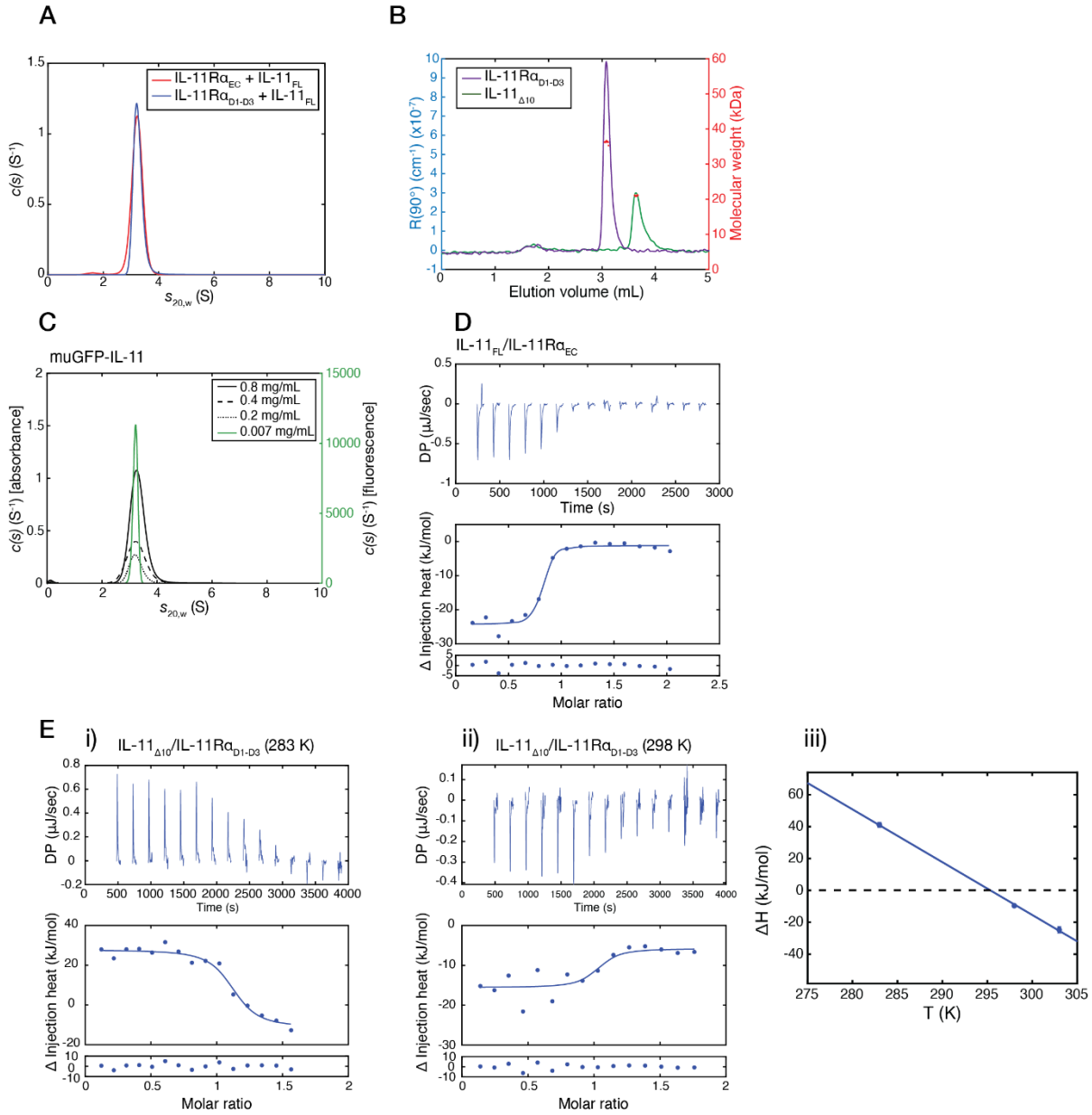

Figure S6: Biophysical characterization of muGFP-IL-11 and the IL-11/IL-11Rα complex. A) c(s) distribution for the complexes formed between IL-11_{FL} and IL-$11R\alpha_{ECD}$, and IL-11_{FL} and IL-$11R\alpha_{D1\text{-}D3}$. The complexes were formed by mixing 5 µM IL-11 and IL-11Rα prior to the experiment, with no further purification. B) SEC-MALS chromatograms (showing light scattering at 90 ° against elution volume) and molecular weight traces for IL-$11_{\Delta 10}$ (M_w 21.0 kDa), and IL-$11R\alpha_{D1\text{-}D3}$ (M_w 36.3 kDa). C) c(s) distributions for muGFP-IL-11 at four concentrations measured using both absorbance (black) and fluorescence (green) detection, showing that it is monomeric in solution. D) Isothermal titration calorimetry isotherm for the interaction between IL-11_{FL} and IL-$11R\alpha_{EC}$. The K_D was 55 ± 8 nM (n=3 titrations, representative titration shown). E) Measurement of ΔC_p for the IL-$11_{\Delta 10}$/IL-$11R\alpha_{D1\text{-}D3}$ interaction. Titrations at two additional temperatures are shown in i), 283 K and ii) 298 K. The heat capacity plot is shown in iii).

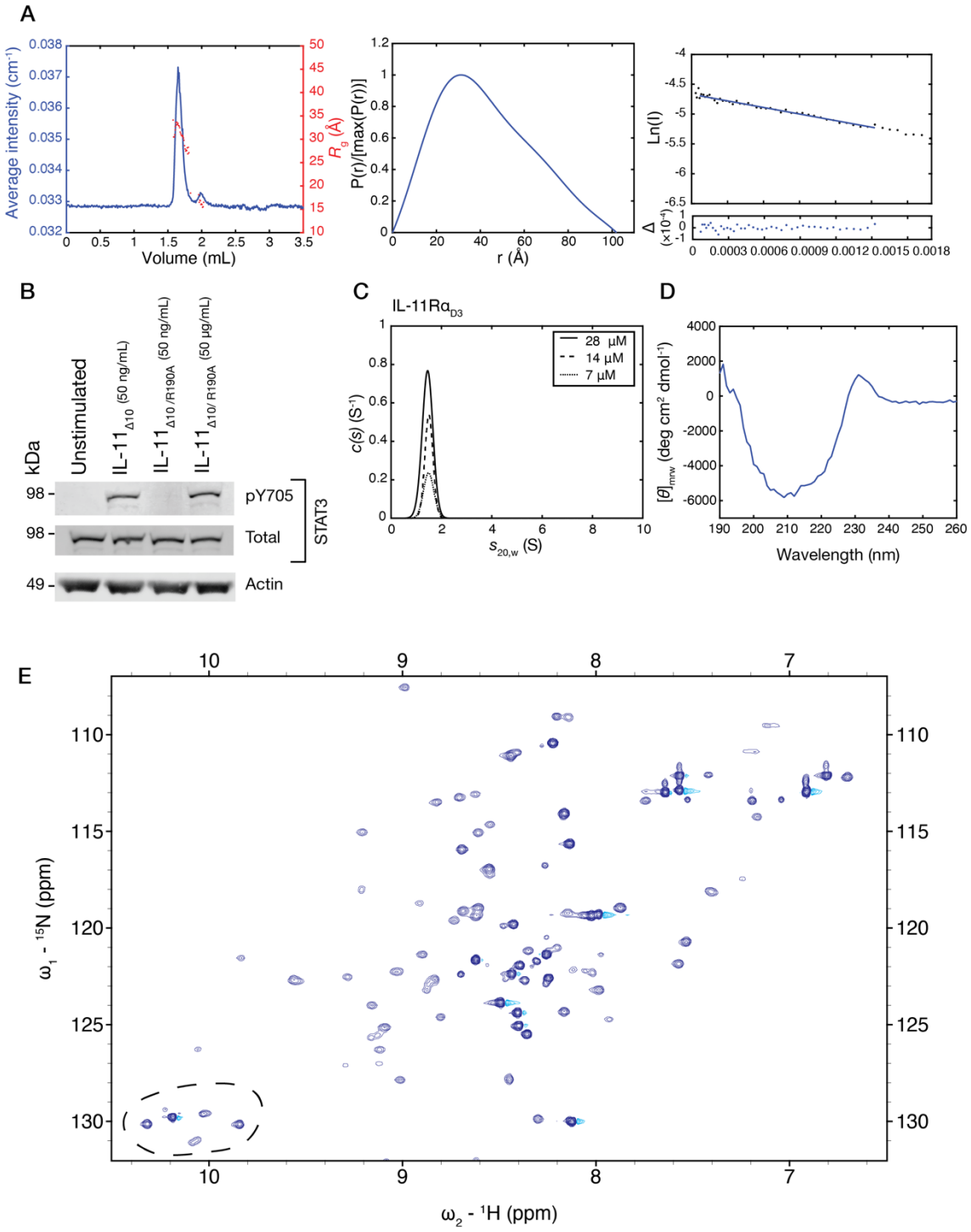

Figure S7: A) SEC-SAXS chromatogram, pairwise distance distribution (P(r)) plot, and Guinier plot for the IL-11$_{\Delta10}$/IL-11Rα$_{D1\text{-}D3}$ complex data shown in Figure 5C. B) Western blot, showing activation of STAT3 by both IL-11$_{\Delta10}$ and IL-11$_{\Delta10/R169A}$ in the colon cancer cell line DLD1. Complete membrane images are shown in Figure S10B. C) CD spectrum for IL-11Rα D3, showing a characteristic all-β spectrum, showing the protein is well folded. D) c(s) distributions for IL-11Rα$_{D3}$ at three concentrations, showing that it is monomeric in solution. E) ^{15}N-^{1}H HSQC spectrum of purified, refolded IL-11Rα$_{D3}$. The spectrum was collected on 130 µM ^{15}N-IL-11Rα$_{D3}$ in 20 mM bis-tris, 50 mM arginine, 10% $^{2}H_2O$, pH 7. Of 108 predicted backbone amide peaks, 93 peaks are observed. Tryptophan indole NH resonances are indicated by the dashed outline.

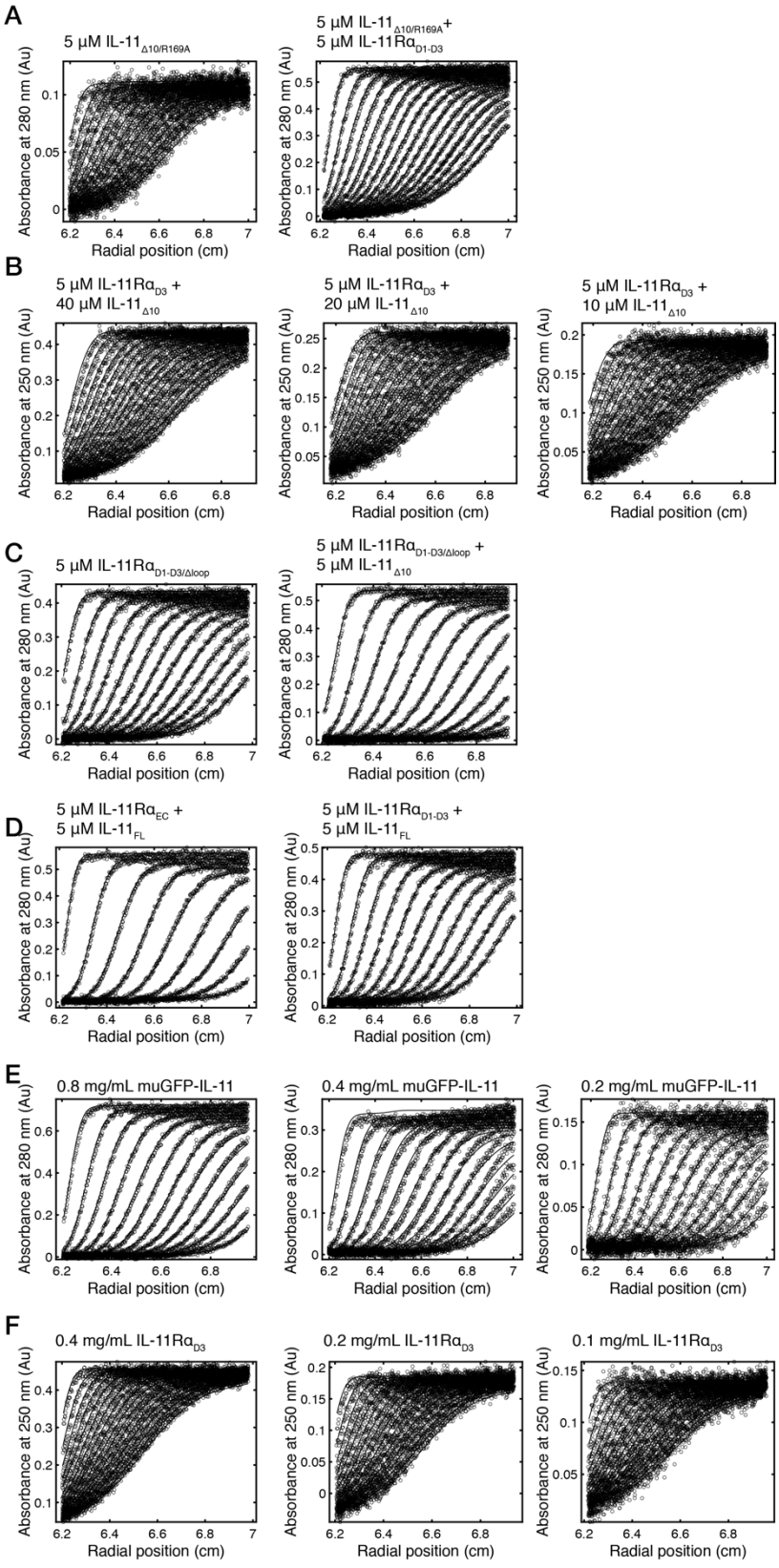

Figure S8: Raw AUC data (circles) overlaid with the best fit to a continuous size distribution [c(s)] model for the distributions shown in, A) Figure 5D ,B) Figure 5E, C) Figure 5F, D) Figure S6A, E) Figure S6B, F) Figure S7D.

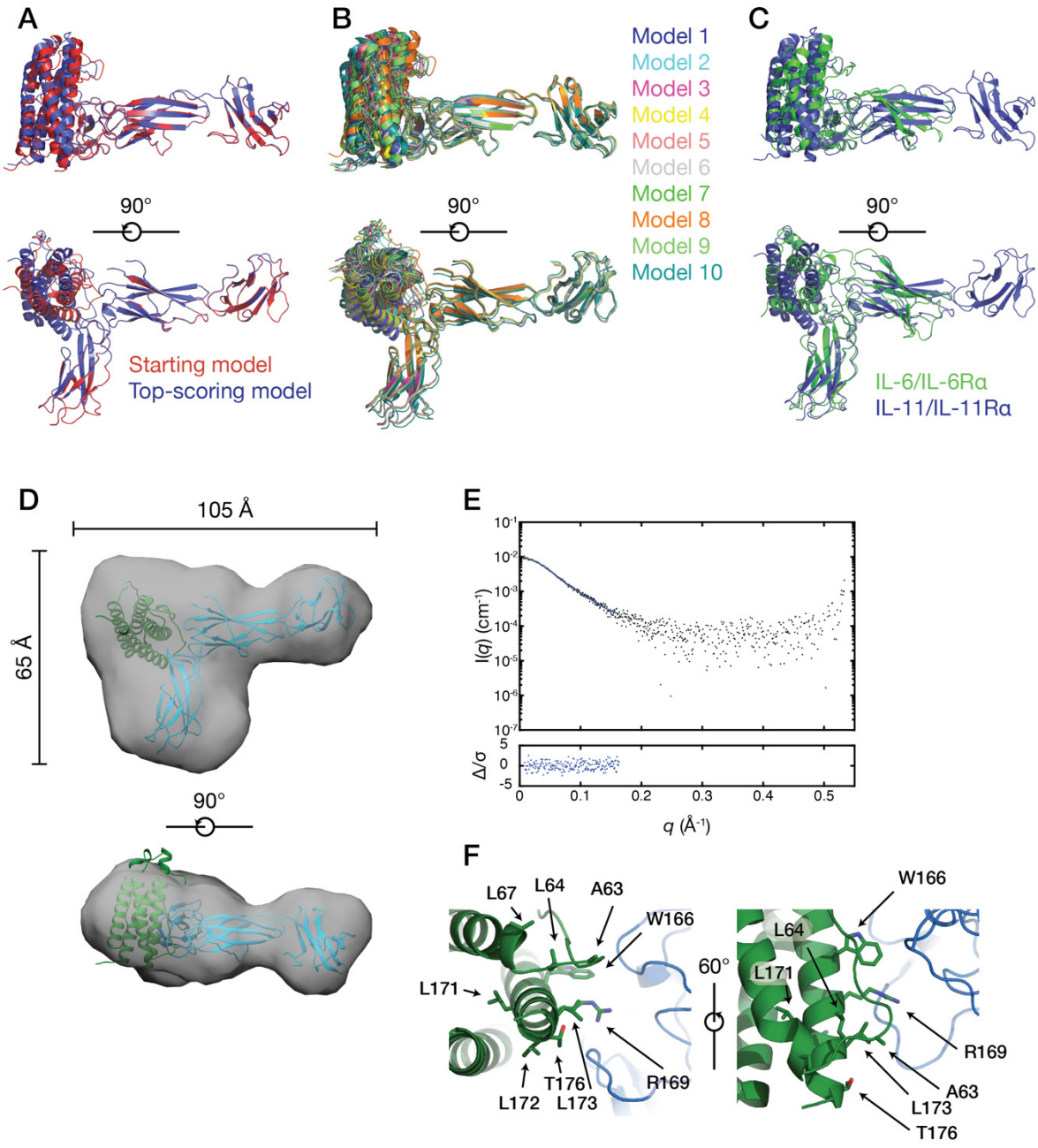

Figure S9: A) Overlay of final, top-scoring docked model and initial starting model. B) Overlay of top ten scoring docked models. C) Overlay of top-scoring model with the crystal structure of the IL-6/IL-6Rα complex (PDB ID: 1P9M) (5). D) *Ab initio* model of the IL-11Rα$_{D1\text{-}D3}$/IL-11$_{\Delta 10}$ complex. (calculated using *DAMMIN*, see Methods), overlaid with the docked model. E) the fit of the *DAMMIN* model to the data (χ^2 = 1.04). F) Position of residues previously studied by mutagenesis (6,7) on the model of the IL-11/IL-11Rα complex.

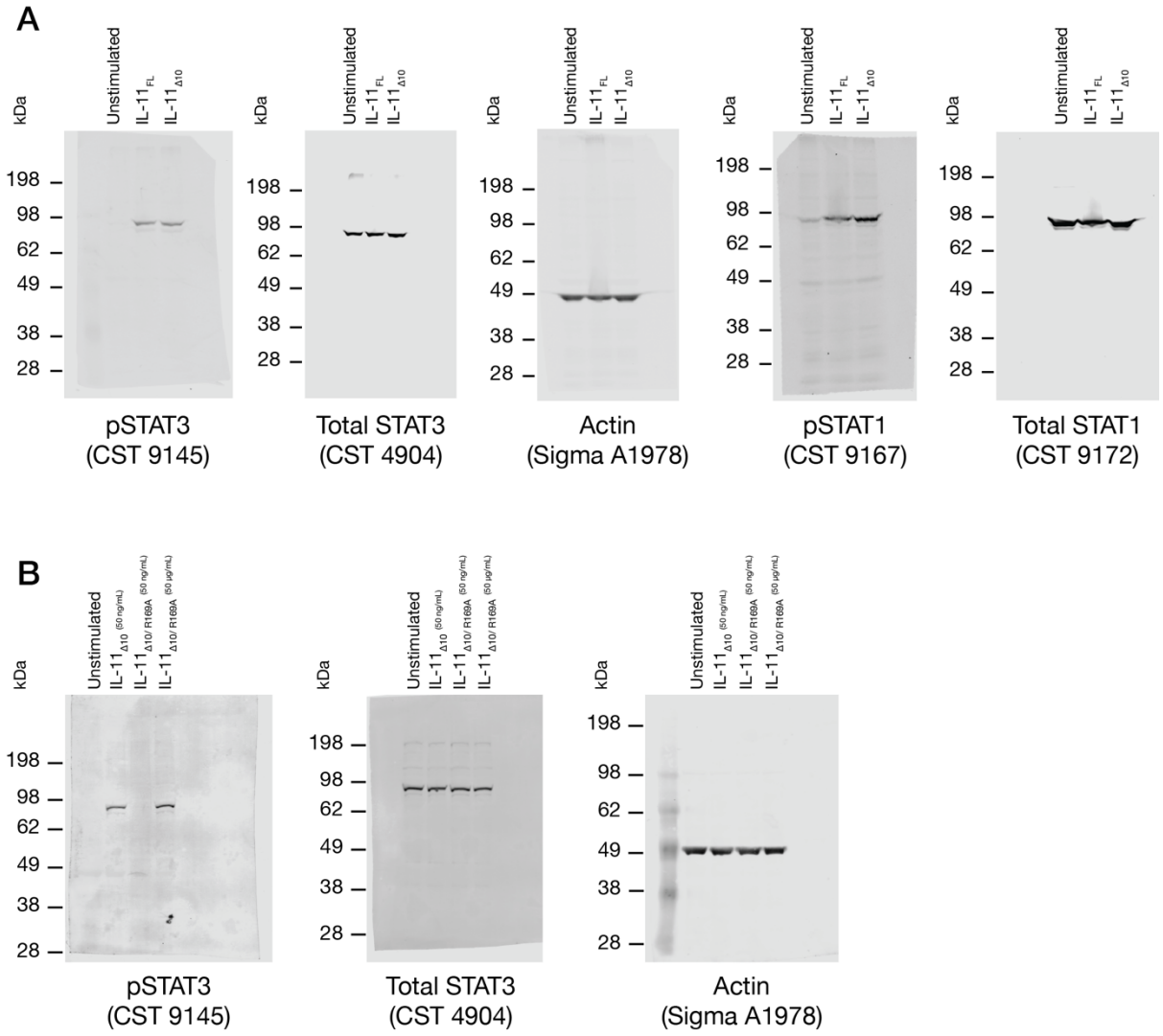

Figure S10: Complete membrane images for, A) the blots shown in Figure 3 and B) the blots shown in Figure S7.

Movie Captions:

Movie S1: Animation of MD simulation of WT IL-11Rα and the IL-11Rα C72F mutant.

Movie S2: Animation of MD simulation of WT IL-11Rα and the IL-11Rα P176T mutant.

Movie S3: Animation of MD simulation of WT IL-11Rα and the IL-11Rα R274W mutant.

Movie S4: Animation of MD simulation of WT IL-11Rα and the IL-11Rα P199R mutant.

Supporting Information References:

1. Rambo, R. P., and Tainer, J. A. (2013) Accurate assessment of mass, models and resolution by small-angle scattering. *Nature* **496**, 477-481
2. Tuukkanen, A. T., Kleywegt, G. J., and Svergun, D. I. (2016) Resolution of ab initio shapes determined from small-angle scattering *IUCrJ* **3**, 440-447
3. Varghese, J., Moritz, R., Lou, M., Van Donkelaar, A., Ji, H., Ivancic, N., Branson, K., Hall, N., and Simpson, R. (2002) Structure of the extracellular domains of the human interleukin-6 receptor α-chain. *P Natl Acad Sci USA* **99**, 15959-15964
4. Chow, D., He, X., Snow, a. L., Rose-John, S., and Garcia, K. C. (2001) Structure of an extracellular gp130 cytokine receptor signaling complex. *Science* **291**, 2150-2155
5. Boulanger, M. J., Chow, D.-c., Brevnova, E. E., and Garcia, K. C. (2003) Hexameric structure and assembly of the interleukin-6/IL-6 alpha-receptor/gp130 complex. *Science* **300**, 2101-2104
6. Tacken, I., Dahmen, H., Boisteau, O., Minvielle, S., Jacques, Y., Grötzinger, J., Küster, A., Horsten, U., Blanc, C., Montero-Julian, F. a., Heinrich, P. C., and Müller-Newen, G. (1999) Definition of receptor binding sites on human interleukin-11 by molecular modeling-guided mutagenesis. *European Journal of Biochemistry* **265**, 645-655
7. Barton, V., Hudson, K. R., and Heath, J. K. (1999) Identification of three distinct receptor binding sites of murine interleukin-11. *Journal of Biological Chemistry* **274**, 5755-5761